PD-1^high^CXCR5⁻CD4⁺ peripheral helper T cells promote CXCR3⁺ plasmablasts in human acute viral infection

Graphical abstract
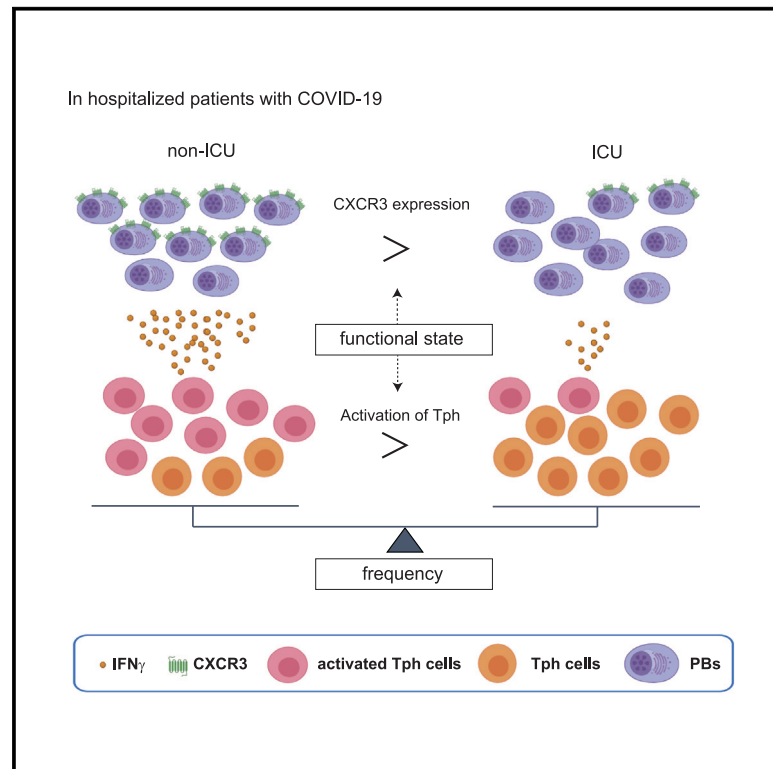
Authors

Hiromitsu Asashima, Subhasis Mohanty, Michela Comi, ..., Albert C. Shaw, David A. Hafler, Tomokazu S. Sumida

Correspondence

tomokazu.sumida@yale.edu

In brief

Asashima et al. report that peripheral helper T cells (denoted as PD-1^high^ CXCR5⁻CD4⁺ T cells) are significantly increased in the acute phase of COVID-19, as are plasmablasts. Plasmablasts show increased *CXCR3* expression, which is induced by IFNγ, and are positively correlated with activated Tph cells with better clinical outcome.

Highlights

- PD-1^high^CXCR5⁻ Tph cells are increased in human acute viral infections

- Expansions of Tph cells and plasmablasts (PBs) are features of early immune responses

- Activated Tph cells and CXCR3⁺ PBs are linked to less severe clinical outcome

- IFNγ from PD-1^high^CXCR5⁻ Tph cells induces CXCR3 expression on PBs

CellPress

Cell Reports

Report

PD-1^{high}CXCR5$^-$CD4$^+$ peripheral helper T cells promote CXCR3$^+$ plasmablasts in human acute viral infection

Hiromitsu Asashima,[1,2] Subhasis Mohanty,[3] Michela Comi,[1,2] William E. Ruff,[1,2] Kenneth B. Hoehn,[4] Patrick Wong,[2] Jon Klein,[2] Carolina Lucas,[2] Inessa Cohen,[1,2] Sarah Coffey,[1,2] Nikhil Lele,[1,2] Leissa Greta,[1,2] Khadir Raddassi,[1,2] Omkar Chaudhary,[3] Avraham Unterman,[5] Brinda Emu,[3] Steven H. Kleinstein,[2,4,6] Ruth R. Montgomery,[7] Akiko Iwasaki,[2,3,8] Charles S. Dela Cruz,[5] Naftali Kaminski,[5] Albert C. Shaw,[3] David A. Hafler,[1,2] and Tomokazu S. Sumida[1,9,*]

[1]Department of Neurology, Yale School of Medicine, New Haven, CT, USA
[2]Department of Immunobiology, Yale School of Medicine, New Haven, CT, USA
[3]Section of Infectious Diseases, Department of Internal Medicine, Yale School of Medicine, Yale University, New Haven, CT, USA
[4]Department of Pathology, Yale School of Medicine, New Haven, CT, USA
[5]Section of Pulmonary, Critical Care and Sleep Medicine Section, Department of Internal Medicine, School of Medicine, Yale University, New Haven, CT, USA
[6]Program in Computational Biology and Bioinformatics, Yale University, New Haven, CT, USA
[7]Department of Internal Medicine, Yale School of Medicine, New Haven, CT, USA
[8]Howard Hughes Medical Institute, Chevy Chase, MD, USA
[9]Lead contact
*Correspondence: tomokazu.sumida@yale.edu
https://doi.org/10.1016/j.celrep.2022.111895

SUMMARY

T cell-B cell interaction is the key immune response to protect the host from severe viral infection. However, how T cells support B cells to exert protective humoral immunity in humans is not well understood. Here, we use COVID-19 as a model of acute viral infections and analyze CD4$^+$ T cell subsets associated with plasmablast expansion and clinical outcome. Peripheral helper T cells (Tph cells; denoted as PD-1^{high}CXCR5$^-$CD4$^+$ T cells) are significantly increased, as are plasmablasts. Tph cells exhibit "B cell help" signatures and induce plasmablast differentiation *in vitro*. Interestingly, expanded plasmablasts show increased *CXCR3* expression, which is positively correlated with higher frequency of activated Tph cells and better clinical outcome. Mechanistically, Tph cells help B cell differentiation and produce more interferon γ (IFNγ), which induces CXCR3 expression on plasmablasts. These results elucidate a role for Tph cells in regulating protective B cell response during acute viral infection.

INTRODUCTION

Severe acute respiratory syndrome coronavirus 2 (SARS-CoV-2) causes a wide spectrum of symptoms ranging from asymptomatic infections to acute respiratory distress syndrome (ARDS).[1,2] COVID-19 is the clinical manifestation of SARS-CoV-2 infection, and it has become clear that a dysregulated immune response against SARS-CoV-2 in the early phase is central for disease severity.[3-6] The generation of a robust antibody response is critical for clearing the virus, and the increase in plasmablasts, which can represent up to 30% of circulating B cells, is observed in a subset of patients with COVID-19 comparable to acute Ebola or dengue virus infections.[7,8]

During the early phase of viral infections, activated B cells differentiate into plasmablasts that migrate to target inflammatory tissues,[9] indicating that the characteristics of plasmablasts are important in the disease course. These plasmablasts express chemoattractant receptors together with adhesion molecules and produce organ-specific protective antibodies for viral

control.[10,11] This rapid antibody response is critical as the early containment of virus reduces the risk of cytokine storm syndrome with excessive accumulation of immune cells in the lung parenchyma with ARDS.[12,13] Recent studies suggested that the rapid generation of neutralizing antibodies is associated with protective immune response in COVID-19.[14,15] Despite this important role of virus-specific antibodies, the control of expansion and chemoattractant receptors of plasmablasts in the early phase of human viral infections remains poorly understood.

During the adaptive immune response, T follicular helper (Tfh) cells play crucial roles in B cell differentiation.[16,17] Circulating CXCR5$^+$CD4$^+$ T cells (cTfh) appear to represent the circulating compartment of Tfh cells.[18] Intriguingly, while the plasmablast response correlates with the cTfh frequency in subjects recovered from COVID-19,[19] that is not the case in the early phase of symptomatic patients with COVID-19.[6] Moreover, Tfh-independent antibody responses are induced against both SARS-CoV-2 and influenza virus infections in mouse models.[20] These data suggest that activated helper T cells other than Tfh cells
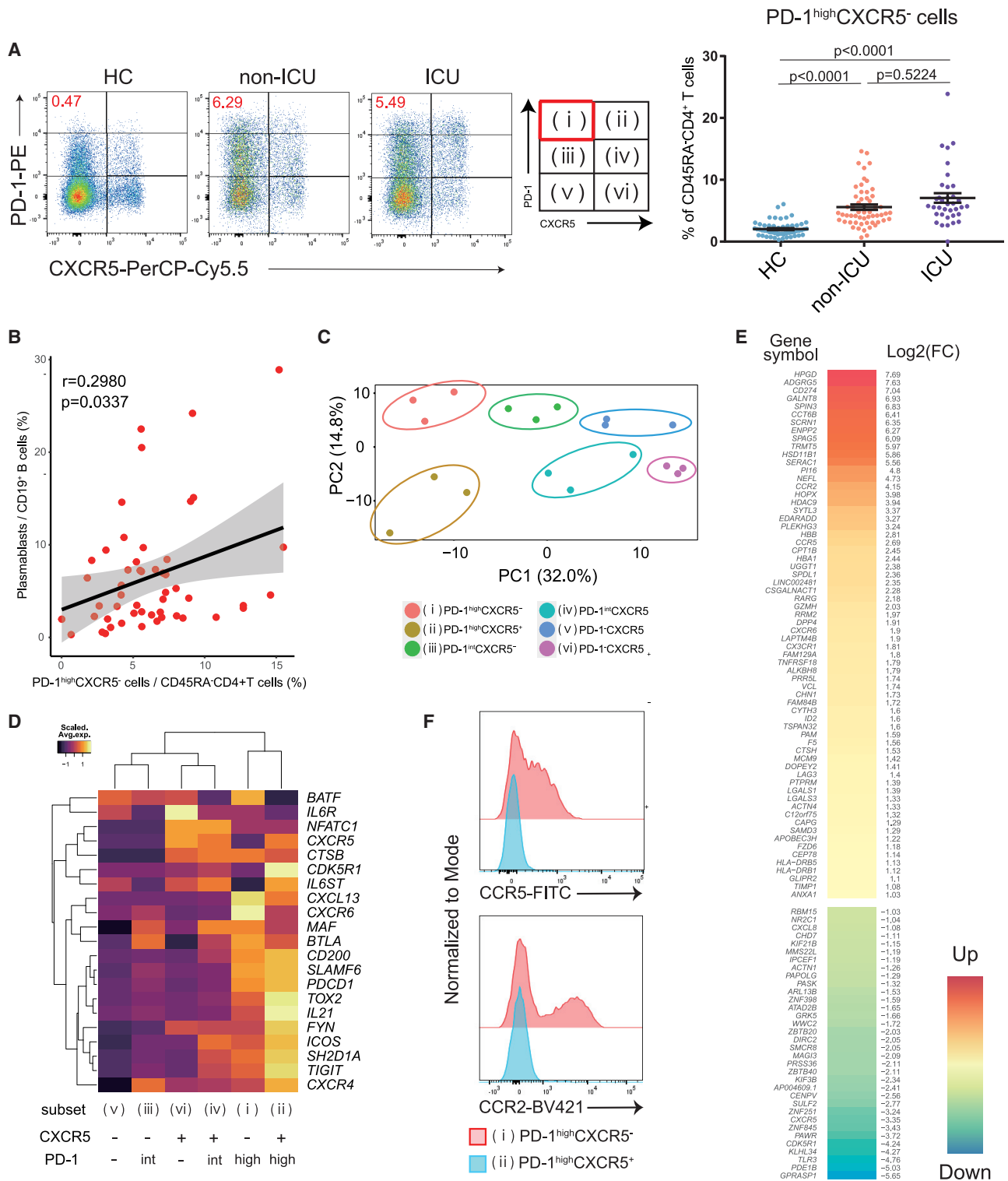
Figure 1. The characteristics of PD-1^{high}CXCR5^− Tph cells

(A) Representative data of PD-1^{high}CXCR5^− Tph cells in each group (left), the proportion of these T cells among healthcare workers (HCs) (n = 55), non-ICU patients with COVID-19 (non-ICU) (n = 56), and ICU patients (ICU) (n = 36). One-way ANOVA with Dunn's multiple comparisons tests were performed (right). Data are represented as mean ± SEM.

(legend continued on next page)

indeed support the differentiation of B cells apart from germinal centers in the early phase of viral infections. However, what subset of T cells induce B cell differentiation in the early phase of human viral infections has not been elucidated.

To explore these mechanisms, we utilized immune profiles of COVID-19 as a model of acute viral infection in human and investigated the characteristics of B and T cells in patients with COVID-19 by integrating single cell RNA-seq (scRNA-seq) and flow cytometry datasets. Here, we report that PD-1^{high}CXCR5$^-$CD4$^+$ T cells, so called peripheral helper T (Tph) cells,[21,22] are significantly increased and positively correlated with the frequency of plasmablasts in peripheral blood in hospitalized patients with COVID-19. These Tph cells exhibit "B cell help" signatures to a similar degree as cTfh cells, but express higher inflammatory chemokine receptors, including *CCR2* and *CCR5,* compared to cTfh cells. *In vitro* experiments indicate that activated PD-1^{high}CXCR5$^-$ Tph cells exhibit higher IFNγ production than activated cTfh cells, which promote CXCR3 expression and differentiation of plasmablasts. Finally, we demonstrate that CXCR3$^+$ plasmablasts are significantly increased in hospitalized patients with less severe disease without ICU admission, while they are decreased in patients admitted to ICU requiring mechanical ventilation. These findings provide a mechanism for the increase of plasmablasts apart from Tfh cells in the early phase of COVID-19, indicating that the induction of CXCR3$^+$ plasmablasts by activated PD-1^{high}CXCR5$^-$ Tph cells is important for disease control. These results elucidate a role for Tph cells in regulating antibody response associated with acute viral infection.

RESULTS

PD-1^{high}CXCR5$^-$Tph cells are significantly increased in the early phase of COVID-19 and have a distinctive gene expression profile

Tfh cells provide essential B cell help, and circulating PD-1$^+$ CXCR5$^+$ Tfh (cTfh) cells appear to represent circulating compartment of Tfh cells.[18,23,24] As noted above, another T cell population expressing high levels of PD-1, but not CXCR5, was recently identified as playing a role in extra-follicular B cell differentiation in autoimmune disorders.[21,22] In addition to an absence of germinal centers in lymphoid organs in the early phase of COVID-19,[25] we hypothesized that PD-1^{high}CXCR5$^-$ Tph cells may drive plasmablast expansion. We first categorized hospitalized patients with COVID-19 into 2 groups based on their admission to the intensive care unit (ICU): hospitalized patients without admission to the ICU (non-ICU subjects), and patients requiring mechanical ventilation in the ICU during hospitalization (ICU subjects) (Table S1). We evaluated CD45RA$^-$CD4$^+$ T cell subsets based on PD-1 and CXCR5

expression and found that PD-1^{high}CXCR5$^-$ Tph cells were significantly increased in patients with COVID-19 and were positively correlated with the frequency of circulating plasmablasts (Figures 1A, 1B, and S1A). Samples were collected on the average of 11.8 days after first symptoms in patients with COVID-19, and there was no significant difference between two groups (non-ICU: 11.7 ± 10.1 days; ICU: 12.3 ± 10.5 days). In contrast, while PD1$^+$CXCR5$^+$ Tfh cells (both PD-1^{high}CXCR5$^+$ Tfh cells and PD-1^{int}CXCR5$^+$ Tfh cells) were also increased in the blood of patients with COVID-19, they were not correlated with plasmablasts in the early phase (Figures S1B–S1D). Moreover, the proportion of PD-1^{high}CXCR5$^-$ Tph cells was not related to clinical characteristics (age, body mass index [BMI], and sex) (Figures S2A–S2C). These observations were replicated by reanalyzing flow cytometry data of patients with COVID-19 from a different study[6] (Figures S3A–S3C).

To further characterize these T helper populations, transcriptional profiles of six subsets of memory CD4$^+$ T cells (CD45RA$^-$ CD4$^+$ T cells), categorized by PD-1 and CXCR5 expression levels, were examined by bulk RNA sequencing (RNA-seq) (Figure 1C). Principal-component analysis (PCA) placed Tph cells at a distinctive position relative to the other subsets. Tph cells express Tfh-related genes *(MAF, TIGIT,* SLAMF6, and *IL21),*[21] which are important for Tfh functions (Figure 1D). PD-1^{int} CXCR5$^+$ Tfh cells also expressed these genes but had less *ICOS* expression than PD-1^{high}CXCR5$^+$ Tfh cells, suggesting that PD-1^{high}CXCR5$^+$ Tfh cells are more activated cTfh cells.[16] We identified 100 genes that were differentially expressed in PD-1^{high}CXCR5$^-$ Tph cells compared with PD-1^{high}CXCR5$^+$ Tfh cells (|log2FC| > 1, FDR < 0.05) (Figure 1E). PD-1^{high}CXCR5$^-$ Tph cells expressed activation markers such as HLA-DRB1 and pathways associated with "cell adhesion molecules," "adheres junctions," and "cytokine-cytokine receptor interaction" were enriched in Tph cells (Figures S2D and S2E). In addition, Tph cells showed marked upregulation of tissue-resident chemokine receptors, including *CCR2, CCR5,* and *CX3CR1* (Figure 1F), and Th1-like signatures *(CXCR3, TBX21,* and *STAT1)* (Figure S2F). Thus, Tph cells exhibit "B cell help" signatures to a similar degree as cTfh cells but with a distinctive gene expression profile.

Activated PD-1^{high}CXCR5$^-$ Tph cells are significantly increased in non-ICU patients and induce plasmablasts *in vitro*

To further evaluate the specific gene signatures of PD-1^{high} CXCR5$^-$ Tph cells, we compared them with the other five subsets in memory CD4$^+$ T cells. *CXCR6, LAG3,* and *PRR5L* were significantly upregulated, while *CHD7, ZBTB20, ZNF251, GRK25,* and *GPRASP1* were significantly downregulated in

(B) Correlation between PD-1^{high}CXCR5$^-$ Tph cells and plasmablasts in patients (both non-ICU and ICU, n = 51). Linear regression is shown with 95% confidence interval (gray area). Correlation statistics is two-tailed Spearman's rank correlation test.

(C) Principal-component analysis (PCA) of RNA-seq transcriptomes (n = 3, patients with COVID-19). Based on the expressions of PD-1 and CXCR5, six subsets were evaluated.

(D) Heatmap of Tfh-related genes.[21]

(E) Clustered heatmap of 100 genes that were differentially expressed (left column) in PD-1^{high}CXCR5$^-$ Tph cells compared with cTfh cells (PD-1^{high}CXCR5$^+$ Tfh cells) (|log2FC| > 1, FDR < 0.05). The right column shows the log2FC.

(F) Representative data of CCR5 and CCR2 expression on PD-1^{high}CXCR5$^-$ Tph cells compared with PD-1^{high}CXCR5$^+$ Tfh cells.
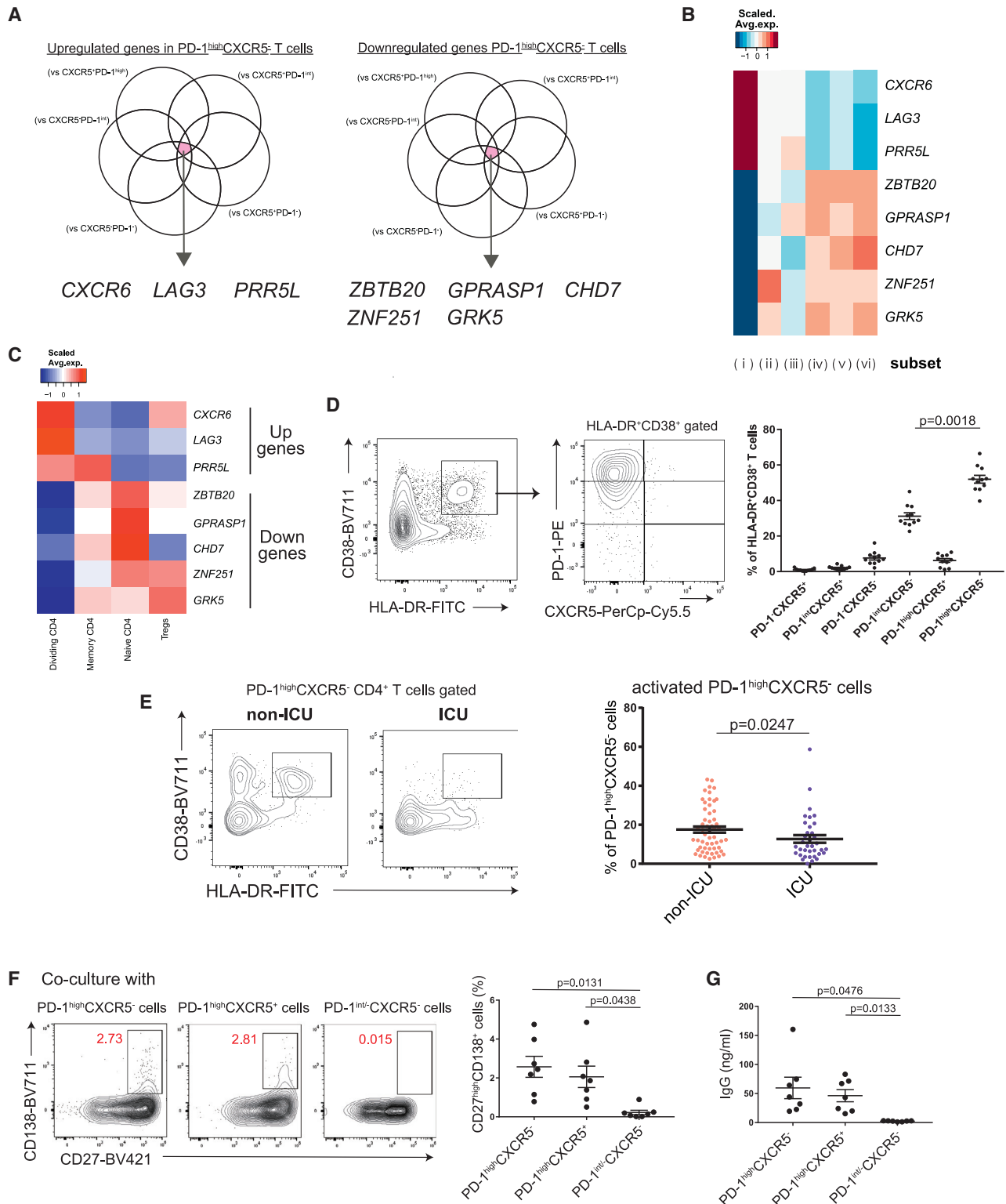
See also Figures S1–S3.

Figure 2. Activated PD-1^highCXCR5⁻ Tph cells are significantly increased in non-ICU patients with COVID-19

(A) Venn diagrams showing the overlapped genes among those significantly upregulated (log2FC > 1, FDR < 0.05) (left) and downregulated (log2FC < −1, FDR < 0.05) (right) in PD-1^highCXCR5⁻ Tph cells compared with five subsets.

(B) Heatmap of PD-1^highCXCR5⁻ Tph cell-related genes (selected in A).

(legend continued on next page)

PD-1[high]CXCR5^{−} Tph cells (Figures 2A and 2B). Flow cytometry analysis also showed the same trend for upregulation of LAG3 and CXCR6 (Figures S4A and S4B). By interrogating these gene lists with CD4^{+} T cell clusters from our single-cell RNA-seq (scRNA-seq) dataset,[5] we found that dividing CD4^{+} T cells best fit with these signatures (Figure 2C). We previously reported that dividing CD4^{+} T cells share the characteristics of HLA-DR^{+}CD38^{+} activated T cells,[5] and indeed, more than half of the activated CD4^{+} T cells fell into the PD-1^{high}CXCR5^{−} Tph cell compartment (Figure 2D). Of note, this activated state of PD-1^{high}CXCR5^{−} Tph cells was significantly increased in the less severely ill non-ICU patients compared with ICU patients (Figure 2E). We confirmed that these observations were not confounded by known risk factors for disease severity such as age, BMI, and sex (Figures S4C–S4E). While there was no difference in the proportion of PD-1^{high}CXCR5^{−} Tph cells between non-ICU and ICU patients at baseline, the expansion of Tph cells was accelerated at the later phase in the more severely ill ICU patients, and the difference reached significance at 2 weeks after the baseline measurement (Figure S4F). In contrast, the higher activation state of PD-1^{high}CXCR5^{−} Tph cells in non-ICU compared with ICU patients at baseline became less significant over time (Figure S4G). These differences were not attributed to the start date of treatment (p = 0.4337; Mann-Whitney test).

In the light of cTfh cells being implicated in the later phase of anti-SARS-CoV-2 antibody production,[19,26,27] we examined whether PD-1^{high}CXCR5^{−} Tph cells promote B cell differentiation *in vitro*. As well as cTfh cells, PD-1^{high}CXCR5^{−} Tph cells helped differentiation of memory B cells into plasmablasts and initiated immunoglobulin G (IgG) production (Figures 2F and 2G). These data suggest that the activated PD-1^{high}CXCR5^{−} Tph cells can support B cell differentiation and that their early induction was associated with better clinical outcome.

The proportion of CXCR3^{+} plasmablasts is positively correlated with that of activated PD-1^{high}CXCR5^{−} Tph cells in the early phase of COVID-19

Next, we evaluated B cell signatures and confirmed that the frequency of plasmablasts is significantly increased in the peripheral blood of patients with COVID-19[3,28] (Figure 3A). Notably, there was no significant difference in the proportion of plasmablasts between non-ICU and ICU groups in hospitalized patients. To further understand the characteristics of B cells in patients with COVID-19, we analyzed our scRNA-seq data[5] and subclustered B cells (total 13,550 cells from 31 samples) into eight clusters (Figures 3B, S5A, and S5B). These samples were collected on the average of 11.7 days after first symptom, and there was

no difference between the two groups in patients with COVID-19 (non-ICU: 11.4 ± 5.9 days, ICU: 12.3 ± 5 days), which was the same as flow cytometry analysis. We identified naive B cells (*MS4A1^{+}IGHD^{+}*); germinal center (GC)-like B cells (*MS4A1^{+}NEIL1^{+}*); intermediate memory B cells (*IGHD^{+}CD27^{+}*); memory B cells (*MS4A1^{+}CD27^{+}*); and two plasma cell clusters, plasmablasts (*MZB1^{+}CD38^{+}*) and Ki67^{+} plasmablasts (*MZB1^{+}CD38^{+}MKI67^{+}*), in accordance with a previous report.[29] Additionally, we were able to identify two more clusters, namely, FCRL5^{+} B cells (*MS4A1^{+}FCRL5^{+}*) and CD1c^{+} B cells (*MS4A1^{+}CD1C^{+}*). FCRL5^{+} B cells also express higher levels of *ITGAX* and *ZEB2* than other B cells, and this cluster was similar with atypical B cells or double-negative (DN) cells[30–32] (Figure S5C). CD1c^{+} B cells express higher levels of *CD52*, which implies that their gene expression signatures resemble marginal zone-like B cells.[33,34] We found that the proportions of two plasmablast clusters within total B cells were not different between non-ICU and ICU subjects, while GC-like B cells was significantly decreased in ICU patients compared with healthy controls (Figure S5D). With regard to B cell receptor (BCR) sequences, both plasmablast clusters expressed IgG, indicating that they had undergone class switching (Figure S6A). While there was no significant difference in the clonal diversity or the frequency of unmutated clones between the two clusters (Figures S6B and S6C), Ki67^{+} plasmablasts showed a significantly lower frequency of somatic hypermutations compared with the other plasmablasts (Figure S6D).

To further examine the characteristics of each cluster identified by scRNA-seq, we assessed the expression of genes that are associated with B cell function[36] (Figure S5E). It was of interest that the expression level of *CXCR3*, the chemoattractant receptor, was upregulated in plasmablast clusters in viral-infected subjects, specifically in the Ki67^{+} plasmablast cluster. In contrast, the homing receptors[35] known to guide immune cells to lymph nodes (*CCR7*, *SELL*) were expressed in healthy control plasmablasts (Figures 3C and 3D). Additionally, we observed a positive correlation between activated PD-1^{high}CXCR5^{−} Tph cells and CXCR3^{+} plasmablasts (Figure 3E). We also evaluated the relationship between activated PD-1[high/int]CXCR5^{+} Tfh cells and CXCR3^{+} plasmablasts, which did not have a significant positive correlation (r = 0.2592, p = 0.0662).

To elucidate the functional readouts with regard to PD-1^{high}CXCR5^{−} Tph cells and CXCR3^{+} plasmablasts, we evaluated anti-SARS-CoV-2 antibodies. The proportion of CXCR3^{+} plasmablasts was positively correlated with the level of SARS-CoV-2 neutralizing antibodies (Figure S7A), and moreover, antibody titers were more correlated with the frequencies of

---

(C) Heatmap of PD-1^{high}CXCR5^{−} Tph cell-related genes (selected in A) among each T cell cluster of our scRNA-seq dataset reported.[5]

(D) Representative data for each T cell subset among HLA-DR^{+}CD38^{+}CD45RA^{−}CD4^{+} T cells (left), and their proportions were evaluated by one-way ANOVA with Dunn's multiple comparisons tests (right). COVID-19 samples that have more than 5% of HLA-DR^{+}CD38^{+} T cells were evaluated (n = 11).

(E) Representative data of HLA-DR^{+}CD38^{+} activated cells in PD-1^{high}CXCR5^{−} Tph cells between non-ICU and ICU patients (left). The proportions of activated PD-1^{high}CXCR5^{−} Tph cells were evaluated (non-ICU; n = 56, ICU; n = 36) by two-tailed unpaired Student's t test (right).

(F and G) Each T cell subset and autologous CD20^{+}CD27^{+} B cells were co-cultured (n = 7, patients with COVID-19). Representative data of CD27^{high}CD138^{+} plasma cells after co-culture (F, left) and the proportion of plasma cells (F, right). IgG concentrations in supernatants were evaluated (G). PD-1[int/−]CXCR5^{−} T cells indicate both PD-1^{int}CXCR5^{−} T cells (subset iii) and PD-1^{−}CXCR5^{−} T cells (v).

Data are represented as mean ± SEM (D–G).

See also Figure S4.

A HC non-ICU ICU

Plasmablasts

B
1 Naive B
2 GC-like B
3 FCRL5+ B
4 Intermediate memory B
5 Memory B
6 CD1c+ B
7 Plasmablasts
8 Ki67+ plasmablasts

D non-ICU ICU FMO

CXCR3+ PBs

C

E
r=0.3092
p=0.0273

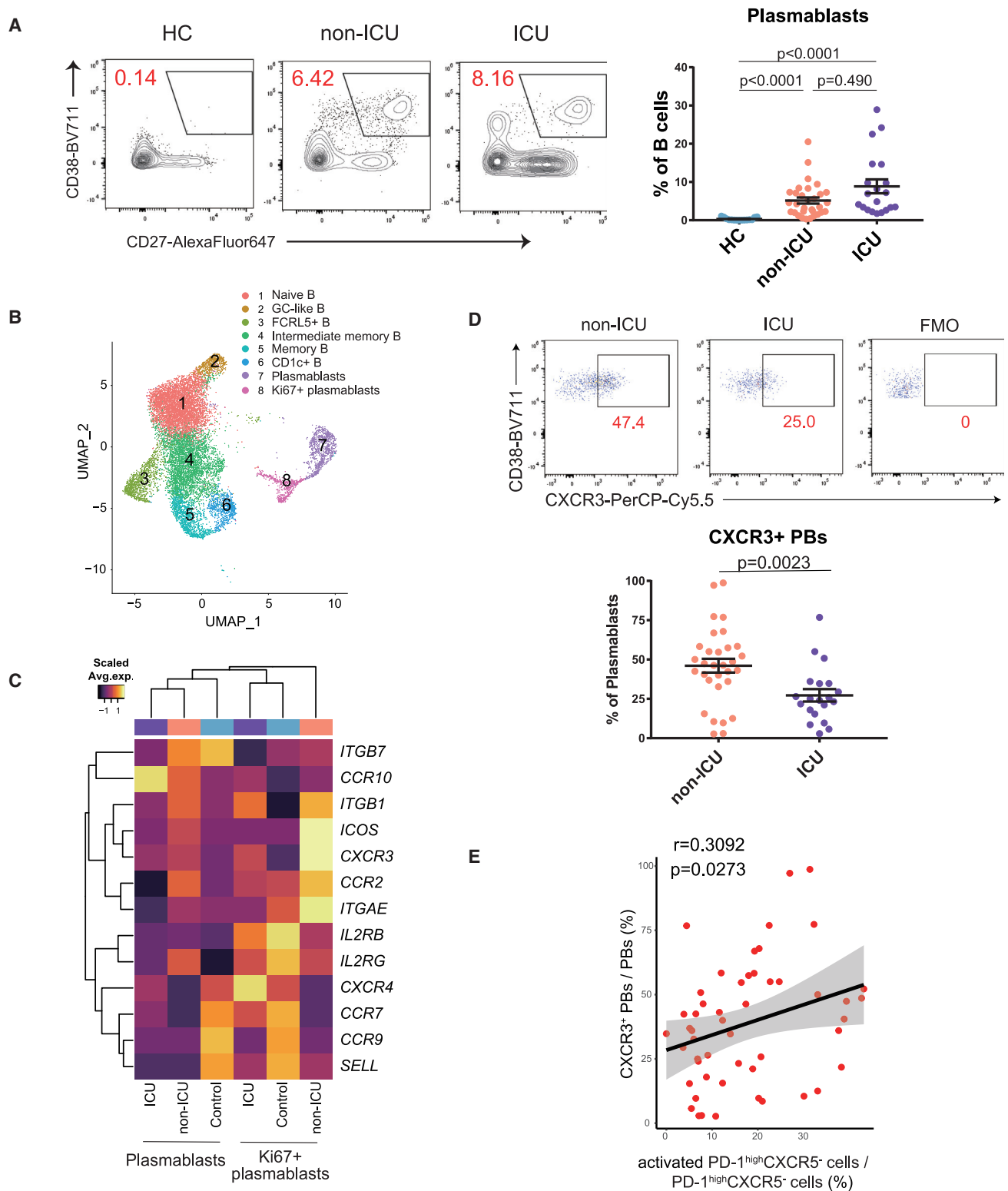activated PD-1^{high}CXCR5$^-$ cells / PD-1^{high}CXCR5$^-$ cells (%)

Figure 3. The divergent immunological features of B cells in non-ICU and ICU patients with COVID-19

(A) Representative data of CD19$^+$CD27$^+$CD38$^+$ plasmablasts (left). Plasmablasts between HCs (n = 15) and non-ICU (n = 31) and ICU patients with COVID-19 (n = 20) were evaluated by one-way ANOVA with Dunn's multiple comparisons tests (right).

activated PD-1^high CXCR5^− Tph cells than those of activated PD-1^+ CXCR5^+ Tfh cells (Figures S7B–S7D).

Taken together, increased CXCR3 expression was one of the features in plasmablasts, and their frequency was positively correlated with that of activated PD-1^high CXCR5^− Tph cells, which might be beneficial in preventing severe viral expansion especially in the early phase.

CXCR3 expression on plasmablasts is induced by higher IFNγ from PD-1^high CXCR5^− Tph cells

To evaluate how CXCR3^+ plasmablasts can be induced by PD-1^high CXCR5^− Tph cells, we examined their cytokine production. Stimulation with anti-CD3/CD28 antibodies induced greater IFNγ and interleukin-10 (IL-10) production from PD-1^high CXCR5^− Tph cells (Figure 4A), which is of interest as IFNγ is known to upregulate *CXCR3* expression during B cell differentiation.[37] We confirmed that PD-1^high CXCR5^− Tph cells produced IL-21 and CXCL13 to the same degree as PD-1^high CXCR5^+ Tfh cells (Figure 4B). We also observed that *CXCR3* expression on plasmablasts was upregulated by IFNγ in a dose-dependent manner, while IL-10 was not (Figures 4C and 4D). In fact, the addition of anti-IFNγ blocking antibodies diminished Tph cell-mediated differentiation of CXCR3^+ plasmablasts *in vitro* (Figure 4E). Moreover, other chemoattractant receptors such as *CCR2* were upregulated besides *CXCR3*, but *CXCR4* was not (Figure 4F). These data indicate that IFNγ produced by PD-1^high CXCR5^− Tph cells induces CXCR3 expression on plasmablasts.

DISCUSSION

PD-1^high CXCR5^− Tph cells were first described in the synovial fluid of rheumatoid arthritis and the peripheral blood of patients with systemic lupus erythematosus (SLE),[21,38] indicating an important role in autoimmune diseases with tissue-specific, ectopic antibody production. Here, we analyzed T cells and B cells in patients with COVID-19 and demonstrated that in the early phase of COVID-19, PD-1^high CXCR5^− Tph cells, exhibiting "B cell help" signatures and promoting B cell differentiation *in vitro*, were significantly increased in hospitalized patients, with COVID-19 correlating with frequencies of plasmablasts. Furthermore, PD-1^high CXCR5^− Tph cells produced more IFNγ, which induced CXCR3 on plasmablasts, and they were correlated with increases in activated Tph cells and anti-SARS-CoV-2 neutralizing antibodies, which were significantly decreased in ICU patients on mechanical ventilation. These results elucidate a role for Tph cells in promoting CXCR3^+ plasmablasts by secre-

tion of IFNγ and in regulating antibody responses associated with viral infection.

Our data demonstrate that not only cTfh cells but also Tph cells play an important role in supporting the expansion of plasmablasts during acute viral infection. One of the common features between the early phase of COVID-19 and chronic autoimmune conditions such as SLE is type-1 IFN (IFN-I) signatures.[5,39,40] IFN-I downregulates CXCR5 expression and upregulates PD-1 expression in human T cells *in vitro*.[41,42] Intriguingly, many differentially expressed genes on Tph cells such as *CXCR6*, *LAG3*, *ZBTB20*, and *CHD7* seem to be regulated by IFN-I in human T cells,[42] indicating that IFN-I might be contributing to Tph cell differentiation.

The antibody responses against infected bacteria are established by day 3 through 5 weeks.[43] However, GC formation was observed approximately 1 month after infection; therefore, antibody responses at the early phase were not GC dependent. In fact, antibodies with low frequencies of somatic hypermutation are detected in the acute viral infections before GC formation and play protective roles against viral infection.[13,44,45] Similarly, in blood from patients with COVID-19, earlier antibody responses are likely to be associated with better recovery.[14,15,46] Our findings that the rapid induction of CXCR3^+ plasmablasts was linked with both a better outcome of disease and the production of protective antibodies support these data. Additionally, we demonstrated that PD-1^high CXCR5^− Tph cells in the activated state support the induction of CXCR3^+ plasmablasts, and these T cells were significantly increased in less severe, non-ICU patients at earlier stages. The significant difference in the frequency of activated PD-1^high CXCR5^− Tph cells between non-ICU and ICU patients waned over time, indicating that the prompt induction of activated PD-1^high CXCR5^− Tph cells might be critical for the promotion of CXCR3^+ plasmablasts and the production of subsequent neutralizing antibodies to effectively remove virus linked with better clinical outcomes. These data provide evidence for the function of activated Tph cells by providing a protective role in the early phase of hospitalized patients with COVID-19, whereas the stronger and delayed/prolonged activation of T cells is known to be associated with worse clinical outcomes.[6] Not only sex differences[3] but also genetic backgrounds are reported to be related to T cell activation,[47,48] and further analyses combined with these factors will lead to the more precise identification of patients at higher risk and are thus expected to be valuable for the development of personalized treatments.

Tph cells are implicated in the extra-follicular B cell responses,[22] and a recent study reported that extra-follicular B cell activation was observed in severe patients with COVID-19,[49] which is seemingly contradictory to our results. However,

(B) Uniform manifold approximation and projection (UMAP) representation of subclustered B cells from HCs (n = 13) and COVID-19 samples (n = 18 from 10 patients).
(C) Heatmap of chemoattractant receptors[36] among HCs and non-ICU and ICU patients with COVID-19 in clusters of both plasmablasts and Ki67^+ plasmablasts. Average expression per subject is shown.
(D) Representative data of CXCR3 expression on CD19^+ CD27^+ CD38^+ plasmablasts in patients with COVID-19 (left). CXCR3^+ plasmablasts between non-ICU (n = 31) and ICU (n = 20) patients with COVID-19 were evaluated by two-tailed unpaired Student's t test (right). FMO, fluorescence minus one.
(E) Correlation between activated PD-1^high CXCR5^− Tph cells and CXCR3^+ plasmablasts (both non-ICU and ICU, n = 51). Linear regression is shown with 95% confidence interval (gray area). Correlation statistics is two-tailed Spearman's rank correlation test.
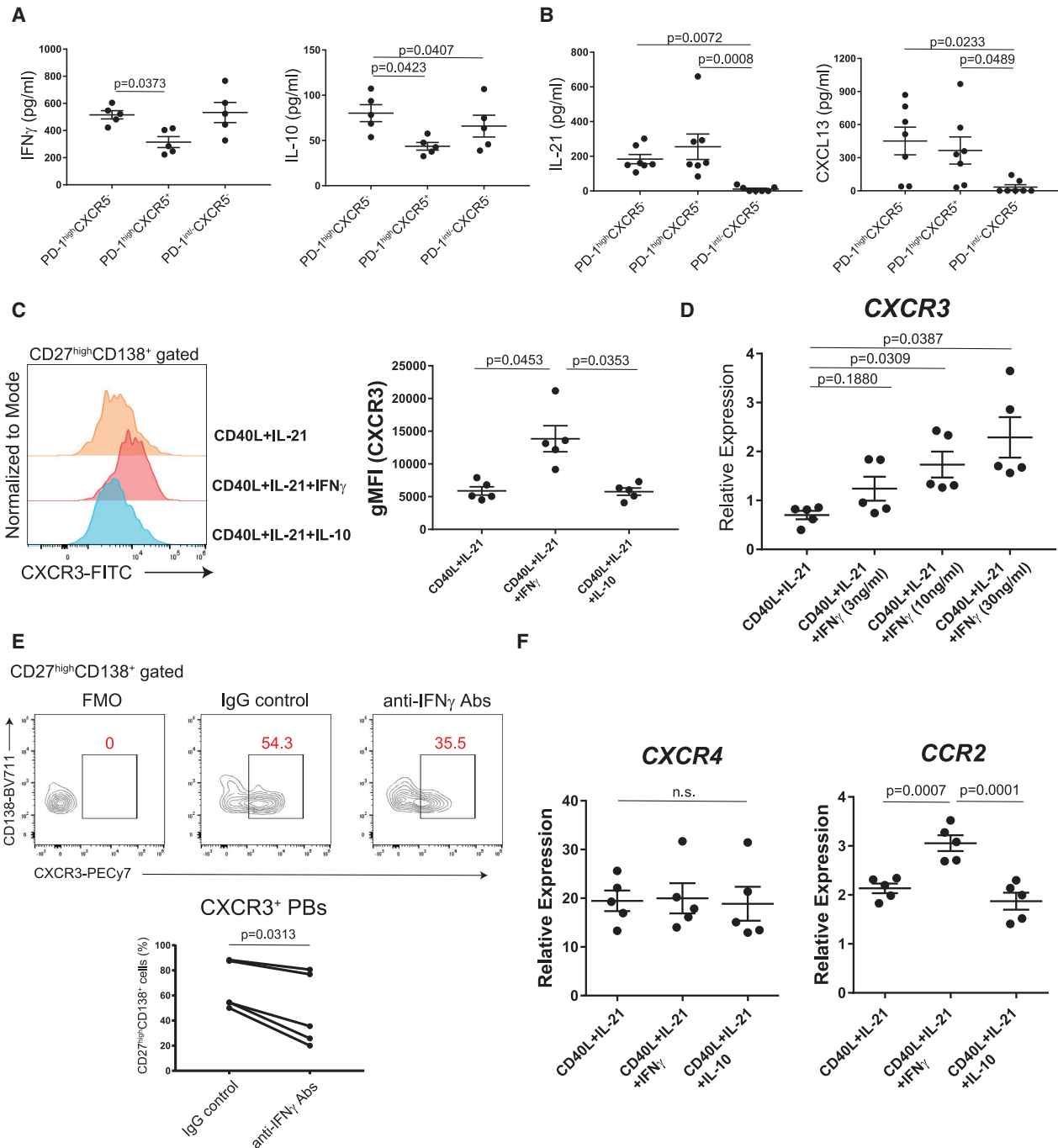Data are represented as mean ± SEM (A and D).
See also Figures S5–S7.

Figure 4. CXCR3 expression on plasmablasts is induced by via IFNγ from PD-1^high^CXCR5^−^ Tph cells

(A) T cells (n = 5, patients with COVID-19) were stimulated with anti-CD3/28 for 48 h, then cytokine productions were measured (IFNγ, IL-10) by ELISA.

(B) IL-21 and CXCL13 levels in the supernatants of co-cultures were measured by ELISA (n = 7, patients with COVID-19).

(C and D) CD20^+^CD27^+^ memory B cells (n = 5, healthy controls) were cultured with CD40L, IL-21, and IL-10 or different concentrations of IFNγ for 7 days (n = 5, healthy controls). Representative histogram for CXCR3 expression on plasma cells (C, left) and CXCR3 gMFI was evaluated (C, right). After 7 days in culture, CD19^+^CD27^+^CD138^+^ plasma cells were sorted, and CXCR3 expression was measured by qPCR (D).

(E) Representative data of CXCR3 expression on CD27^high^CD138^+^ plasma cells after co-culture with Tph cells (n = 5, patients with COVID-19) with anti-human IFNγ antibodies (anti-IFNγ Abs) or IgG isotype controls (IgG control) (E, top). CXCR3^+^CD27^high^CD138^+^ plasma cells (bottom) were evaluated by Wilcoxon matched-pairs signed rank test (E, bottom).

(F) After 7 days culture of CD20^+^CD27^+^ memory B cells (n = 5, healthy donors) with various conditions, gene expressions of CD19^+^CD27^high^CD138^+^ plasma cells were measured by qPCR (n = 5, healthy controls).

Data were evaluated by one-way ANOVA with Tukey's multiple comparisons tests (A–D and F). Data are represented as mean ± SEM (A–D and F).

the categorization of disease severity was different between these studies. The previous study defined the severity based on the hospitalization so that all non-hospitalized patients (i.e., outpatients) were grouped as mild and all hospitalized patients as severe. In contrast, we studied only hospitalized patients and divided inpatients into either a non-ICU cohort or an ICU cohort with severe disease requiring mechanical ventilation or death. Thus, while these clinical categories have some degree of variability, our results nevertheless support previous findings that extra-follicular features are detected in hospitalized patients.

The temporal dynamics of T cell-B cell interaction is crucial to understand immune response during the disease progression of COVID-19. We demonstrated a relationship between PD-1^{high} CXCR5$^-$ Tph cells and CXCR3$^+$ plasmablasts in the acute phase, especially within 14 days after symptom onset. In contrast, Tfh cells play a central role during the recovery phase of COVID-19.[19,27] Recently, Koutsakos et al.[26] identified a correlation between antibody titers and the proportion of cTfh1 cells in patients with COVID-19. However, the dynamics of rapid expansion of plasmablasts, peaking between 1 and 2 weeks from symptom onset, and the gradual increase of cTfh1 cells peaking in 3–4 weeks implicates that T cells other than cTfh1 cells support the rapid expansion of plasmablasts at the earlier phase. Indeed, the PD-1^{high}CXCR5$^+$ T cells with the highest CXCR3 expression (subset 2 in Figure 1A), which correspond to most of cTfh1 cells, were not positively correlated with plasmablast expansion (Figure S3C). Thus, our findings suggest that PD-1^{high}CXCR5$^-$ Tph cells play a major role in the rapid expansion of plasmablasts in the acute phase of hospitalized patients with COVID-19. Subsequently, the transition of "B cell help" T cell population from Tph cells to Tfh cells could shift T cell-B cell interaction from extra-follicular to a GC response that governs long-lasting humoral immunity.

In summary, our data implicate PD-1^{high}CXCR5$^-$ Tph cells as triggering the induction of CXCR3$^+$ plasmablasts via IFNγ in the early phase of acute viral infection by using COVID-19 as an *in vivo* model of human viral infection. These data provide a potential framework for assessing immune response to pathogenic virus and other IFN-I-inducing viral infections. Moreover, these data shed light as to how T cells can drive B cell differentiation in acute viral infections and provide potential insights into the role of PD-1^{high}CXCR5$^-$ Tph cells on a variety of immune-mediated diseases with the possible contribution of aberrant T-B interaction, including chronic autoimmune diseases.

Limitations of the study

Although we performed a bidirectional analysis between T cells and B cells in blood, we could not directly assess the lymphoid tissue samples. Moreover, given that the definition of Tph cells is based on PD1^{high}CXCR5$^-$ memory CD4$^+$ T cells, the functional overlaps between Tph cells and PD-1^{high} Th1 cells are not clear. To decipher the relationship among PD-1^{high}CXCR5$^-$ Tph cells, cTfh1 cells, and PD-1^{high}Th1 cells from the perspective of "B cell help" functions, the spatial interactions between those T cells and B cells at tissue sites can be assessed in future studies. Another limitation is that we could not evaluate the antigen specificity of Tph cells because of limited samples and cell numbers

from patients with COVID-19 who have vaccine- and past-infection-free status. The use of a SARS-CoV-2-specific tetramer with genotyping would have been useful and will be performed in future investigations. In addition, both Tph cells and plasmablasts are small subsets in total lymphocytes, and the assessment of absolute population numbers would have been more helpful. Although our finding highlights the potential role of CXCR3$^+$ plasmablasts during acute viral infection, the functional differences between CXCR3$^+$ and CXCR3$^-$ plasmablasts were not addressed, which is challenging in human but can be clarified by *in vivo* models with Cxcr3 conditional knockout mice. Finally, our correlative data between Tph cells and plasmablasts may reflect the general kinetics of acute viral response and does not necessarily imply that these cells are interdependent. To clarify those causal interactions between Tph cells and plasmablasts *in vivo*, further investigation using murine models is warranted.

STAR★METHODS

Detailed methods are provided in the online version of this paper and include the following:

- KEY RESOURCES TABLE
- RESOURCE AVAILABILITY
  - Lead contact
  - Materials availability
  - Data and code availability
- EXPERIMENTAL MODELS AND SUBJECT DETAILS
  - Ethics Statement
  - Patients and samples
- METHOD DETAILS
  - Peripheral blood mononuclear cells isolation
  - Flow cytometry and sorting
  - T-B-cell co-culture experiments
  - B cell differentiation *in vitro*
  - T cell stimulation *in vitro*
  - Quantitative PCR
  - The measurement of anti-SARS-CoV-2 antibodies
  - Single cell RNA-seq data processing
  - B cell receptor repertoire analysis
  - Bulk RNA-seq
- QUANTIFICATION AND STATISTICAL ANALYSIS

AUTHOR CONTRIBUTIONS

Overall study design, H.A., D.A.H., and T.S.S.; biospecimen collection/processing, H.A., S.M., M.C., W.E.R., P.W., J.K., C.L., K.R., O.C., A.U., B.E., R.R.M., A.I., A.C.S., and T.S.S.; data analysis, H.A., W.E.R., K.B.H., I.C., S.C., N.L., L.G., S.H.K., and T.S.S.; original draft writing, H.A.; supervising the study, D.A.H. and T.S.S.; reviewing and editing the manuscript, all authors.

DECLARATION OF INTERESTS

REFERENCES

1. Wu, Z., and McGoogan, J.M. (2020). Characteristics of and important lessons from the coronavirus disease 2019 (COVID-19) outbreak in China: summary of a report of 72314 cases from the Chinese center for disease control and prevention. JAMA *323*, 1239–1242. https://doi.org/10.1001/jama.2020.2648.

2. Zhu, N., Zhang, D., Wang, W., Li, X., Yang, B., Song, J., Zhao, X., Huang, B., Shi, W., Lu, R., et al. (2020). Novel coronavirus from patients with Pneumonia in China, 2019. N. Engl. J. Med. *382*, 727–733. https://doi.org/10.1056/NEJMoa2001017.

3. Takahashi, T., Ellingson, M.K., Wong, P., Israelow, B., Lucas, C., Klein, J., Silva, J., Mao, T., Oh, J.E., Tokuyama, M., Lu, P., Venkataraman, A., Park, A., Liu, F., Meir, A., Sun, J., Wang, E.Y., Casanovas-Massana, A., Wyllie, A.L., Vogels, C.B.F., Earnest, R., Lapidus, S., Ott, I.M., Moore, A.J., Yale IMPACT Research Team; Shaw, A., Fournier, J.B., Odio, C.D., Farhadian, S., Dela Cruz, C., Grubaugh, N.D., Schulz, W.L., Ring, A.M., Ko, A.I., Omer, S.B., and Iwasaki, A. (2020). Sex differences in immune responses that underlie COVID-19 disease outcomes. Nature *588*, 315–320. https://doi.org/10.1038/s41586-020-2700-3.

4. Giamarellos-Bourboulis, E.J., Netea, M.G., Rovina, N., Akinosoglou, K., Antoniadou, A., Antonakos, N., Damoraki, G., Gkavogianni, T., Adami, M.E., Katsaounou, P., et al. (2020). Complex immune dysregulation in

5. Unterman, A., Sumida, T.S., Nouri, N., Yan, X., Zhao, A.Y., Gasque, V., Schupp, J.C., Asashima, H., Liu, Y., Cosme, C., et al. (2022). Single-cell multi-omics reveals dyssynchrony of the innate and adaptive immune system in progressive COVID-19. Nat. Commun. *13*, 440. https://doi.org/10.1038/s41467-021-27716-4.

6. Mathew, D., Giles, J.R., Baxter, A.E., Oldridge, D.A., Greenplate, A.R., Wu, J.E., Alanio, C., Kuri-Cervantes, L., Pampena, M.B., D'Andrea, K., et al. (2020). Deep immune profiling of COVID-19 patients reveals patient heterogeneity and distinct immunotypes with implications for therapeutic interventions. Science *369*, eabc8511. https://doi.org/10.1126/science.abc8511.

7. McElroy, A.K., Akondy, R.S., Davis, C.W., Ellebedy, A.H., Mehta, A.K., Kraft, C.S., Lyon, G.M., Ribner, B.S., Varkey, J., Sidney, J., et al. (2015). Human Ebola virus infection results in substantial immune activation. Proc. Natl. Acad. Sci. USA *112*, 4719–4724. https://doi.org/10.1073/pnas.1502619112.

8. Wrammert, J., Onlamoon, N., Akondy, R.S., Perng, G.C., Polsrila, K., Chandele, A., Kwissa, M., Pulendran, B., Wilson, P.C., Wittawatmongkol, O., et al. (2012). Rapid and massive virus-specific plasmablast responses during acute dengue virus infection in humans. J. Virol. *86*, 2911–2918. https://doi.org/10.1128/JVI.06075-11.

9. Alon, R., Sportiello, M., Kozlovski, S., Kumar, A., Reilly, E.C., Zarbock, A., Garbi, N., and Topham, D.J. (2021). Leukocyte trafficking to the lungs and beyond: lessons from influenza for COVID-19. Nat. Rev. Immunol. *21*, 49–64. https://doi.org/10.1038/s41577-020-00470-2.

10. Kunkel, E.J., and Butcher, E.C. (2003). Plasma-cell homing. Nat. Rev. Immunol. *3*, 822–829. https://doi.org/10.1038/nri1203.

11. Nutt, S.L., Hodgkin, P.D., Tarlinton, D.M., and Corcoran, L.M. (2015). The generation of antibody-secreting plasma cells. Nat. Rev. Immunol. *15*, 160–171. https://doi.org/10.1038/nri3795.

12. Lerner, R.A. (2011). Rare antibodies from combinatorial libraries suggests an S.O.S. component of the human immunological repertoire. Mol. Biosyst. *7*, 1004–1012. https://doi.org/10.1039/c0mb00310g.

13. Murin, C.D., Wilson, I.A., and Ward, A.B. (2019). Antibody responses to viral infections: a structural perspective across three different enveloped viruses. Nat. Microbiol. *4*, 734–747. https://doi.org/10.1038/s41564-019-0392-y.

14. Lucas, C., Klein, J., Sundaram, M.E., Liu, F., Wong, P., Silva, J., Mao, T., Oh, J.E., Mohanty, S., Huang, J., et al. (2021). Delayed production of neutralizing antibodies correlates with fatal COVID-19. Nat. Med. *27*, 1178–1186. https://doi.org/10.1038/s41591-021-01355-0.

15. Khoury, D.S., Cromer, D., Reynaldi, A., Schlub, T.E., Wheatley, A.K., Juno, J.A., Subbarao, K., Kent, S.J., Triccas, J.A., and Davenport, M.P. (2021). Neutralizing antibody levels are highly predictive of immune protection from symptomatic SARS-CoV-2 infection. Nat. Med. *27*, 1205–1211. https://doi.org/10.1038/s41591-021-01377-8.

16. Ueno, H. (2016). T follicular helper cells in human autoimmunity. Curr. Opin. Immunol. *43*, 24–31. https://doi.org/10.1016/j.coi.2016.08.003.

17. Crotty, S. (2019). T follicular helper cell Biology : a decade of discovery and diseases. Immunity *50*, 1132–1148. https://doi.org/10.1016/j.immuni.2019.04.011.

18. Morita, R., Schmitt, N., Bentebibel, S.E., Ranganathan, R., Bourdery, L., Zurawski, G., Foucat, E., Dullaers, M., Oh, S., Sabzghabaei, N., et al. (2011). Human blood CXCR5(+)CD4(+) T cells are counterparts of T follicular cells and contain specific subsets that differentially support antibody secretion. Immunity *34*, 108–121. https://doi.org/10.1016/j.immuni.2010.12.012.

19. Juno, J.A., Tan, H.X., Lee, W.S., Reynaldi, A., Kelly, H.G., Wragg, K., Esterbauer, R., Kent, H.E., Batten, C.J., Mordant, F.L., et al. (2020). Humoral and circulating follicular helper T cell responses in recovered patients with

COVID-19. Nat. Med. *26*, 1428–1434. https://doi.org/10.1038/s41591-020-0995-0.

20. Chen, J.S., Chow, R.D., Song, E., Mao, T., Israelow, B., Kamath, K., Bozekowski, J., Haynes, W.A., Filler, R.B., Menasche, B.L., et al. (2022). High-affinity, neutralizing antibodies to SARS-CoV-2 can be made without T follicular helper cells. Sci. Immunol. *7*, eabl5652. https://doi.org/10.1126/sciimmunol.abl5652.

21. Rao, D.A., Gurish, M.F., Marshall, J.L., Slowikowski, K., Fonseka, C.Y., Liu, Y., Donlin, L.T., Henderson, L.A., Wei, K., Mizoguchi, F., et al. (2017). Pathologically expanded peripheral T helper cell subset drives B cells in rheumatoid arthritis. Nature *542*, 110–114. https://doi.org/10.1038/nature20810.

22. Yoshitomi, H., and Ueno, H. (2021). Shared and distinct roles of T peripheral helper and T follicular helper cells in human diseases. Cell. Mol. Immunol. *18*, 523–527. https://doi.org/10.1038/s41423-020-00529-z.

23. Locci, M., Havenar-Daughton, C., Landais, E., Wu, J., Kroenke, M.A., Arlehamn, C.L., Su, L.F., Cubas, R., Davis, M.M., Sette, A., et al. (2013). Human circulating PD-1+CXCR3−CXCR5+ memory Tfh cells are highly functional and correlate with broadly neutralizing HIV antibody responses. Immunity *39*, 758–769. https://doi.org/10.1016/j.immuni.2013.08.031.

24. Ueno, H., Banchereau, J., and Vinuesa, C.G. (2015). Pathophysiology of T follicular helper cells in humans and mice. Nat. Immunol. *16*, 142–152. https://doi.org/10.1038/ni.3054.

25. Kaneko, N., Kuo, H.H., Boucau, J., Farmer, J.R., Allard-Chamard, H., Mahajan, V.S., Piechocka-Trocha, A., Lefteri, K., Osborn, M., Bals, J., et al. (2020). Loss of Bcl-6-expressing T follicular helper cells and germinal centers in COVID-19. Cell *183*, 143–157.e13. https://doi.org/10.1016/j.cell.2020.08.025.

26. Koutsakos, M., Rowntree, L.C., Hensen, L., Chua, B.Y., van de Sandt, C.E., Habel, J.R., Zhang, W., Jia, X., Kedzierski, L., Ashhurst, T.M., et al. (2021). Integrated immune dynamics define correlates of COVID-19 severity and antibody responses. Cell Rep. Med. *2*, 100208. https://doi.org/10.1016/j.xcrm.2021.

27. Gong, F., Dai, Y., Zheng, T., Cheng, L., Zhao, D., Wang, H., Liu, M., Pei, H., Jin, T., Yu, D., and Zhou, P. (2020). Peripheral CD4+ T cell subsets and antibody response in COVID-19 convalescent individuals. J. Clin. Invest. *130*, 6588–6599. https://doi.org/10.1172/JCI141054.

28. Lucas, C., Wong, P., Klein, J., Castro, T.B.R., Silva, J., Sundaram, M., Ellingson, M.K., Mao, T., Oh, J.E., Israelow, B., et al. (2020). Longitudinal analyses reveal immunological misfiring in severe COVID-19. Nature *584*, 463–469. https://doi.org/10.1038/s41586-020-2588-y.

29. Zhang, J.Y., Wang, X.M., Xing, X., Xu, Z., Zhang, C., Song, J.W., Fan, X., Xia, P., Fu, J.L., Wang, S.Y., et al. (2020). Single-cell landscape of immunological responses in patients with COVID-19. Nat. Immunol. *21*, 1107–1118. https://doi.org/10.1038/s41590-020-0762-x.

30. Kim, C.C., Baccarella, A.M., Bayat, A., Pepper, M., and Fontana, M.F. (2019). FCRL5+ memory B cells exhibit robust recall responses. Cell Rep. *27*, 1446–1460.e4. https://doi.org/10.1016/j.celrep.2019.04.019.

31. Pérez-Mazliah, D., Ndungu, F.M., Aye, R., and Langhorne, J. (2020). B-cell memory in malaria: myths and realities. Immunol. Rev. *293*, 57–69. https://doi.org/10.1111/imr.12822.

32. Jenks, S.A., Cashman, K.S., Zumaquero, E., Marigorta, U.M., Patel, A.V., Wang, X., Tomar, D., Woodruff, M.C., Simon, Z., Bugrovsky, R., et al. (2018). Distinct effector B cells induced by unregulated toll-like receptor 7 contribute to pathogenic responses in systemic lupus erythematosus. Immunity *49*, 725–739.e6. https://doi.org/10.1016/j.immuni.2018.08.015.

33. Riedel, R., Addo, R., Ferreira-Gomes, M., Heinz, G.A., Heinrich, F., Kummer, J., Greiff, V., Schulz, D., Klaeden, C., Cornelis, R., et al. (2020). Discrete populations of isotype-switched memory B lymphocytes are maintained in murine spleen and bone marrow. Nat. Commun. *11*, 2570. https://doi.org/10.1038/s41467-020-16464-6.

34. Sanz, I., Wei, C., Jenks, S.A., Cashman, K.S., Tipton, C., Woodruff, M.C., Hom, J., and Lee, F.E.H. (2019). Challenges and opportunities for consis-

tent classification of human B cell and plasma cell populations. Front. Immunol. *10*, 2458. https://doi.org/10.3389/fimmu.2019.02458.

35. Pattanapanyasat, K., Khowawisetsut, L., Chuansumrit, A., Chokephaibulkit, K., Tangnararatchakit, K., Apiwattanakul, N., Techasaensiri, C., Thitilertdecha, P., Sae-Ung, T., and Onlamoon, N. (2018). B cell subset alteration and the expression of tissue homing molecules in dengue infected patients. J. Biomed. Sci. *25*, 64. https://doi.org/10.1186/s12929-018-0467-8.

36. Glass, D.R., Tsai, A.G., Oliveria, J.P., Hartmann, F.J., Kimmey, S.C., Calderon, A.A., Borges, L., Glass, M.C., Wagar, L.E., Davis, M.M., and Bendall, S.C. (2020). An integrated multi-omic single-cell atlas of human B cell identity. Immunity *53*, 217–232.e5. https://doi.org/10.1016/j.immuni.2020.06.013.

37. Muehlinghaus, G., Cigliano, L., Huehn, S., Peddinghaus, A., Leyendeckers, H., Hauser, A.E., Hiepe, F., Radbruch, A., Arce, S., and Manz, R.A. (2005). Regulation of CXCR3 and CXCR4 expression during terminal differentiation of memory B cells into plasma cells. Blood *105*, 3965–3971. https://doi.org/10.1182/blood-2004-08-2992.

38. Bocharnikov, A.V., Keegan, J., Wacleche, V.S., Cao, Y., Fonseka, C.Y., Wang, G., Muise, E.S., Zhang, K.X., Arazi, A., Keras, G., et al. (2019). PD-1hiCXCR5– T peripheral helper cells promote B cell responses in lupus via MAF and IL-21. JCI Insight *4*, e130062. https://doi.org/10.1172/jci.insight.130062.

39. Conigliaro, P., Perricone, C., Benson, R.A., Garside, P., Brewer, J.M., Perricone, R., and Valesini, G. (2010). The type I IFN system in rheumatoid arthritis. Autoimmunity *43*, 220–225. https://doi.org/10.3109/08916930903510914.

40. Muskardin, T.L.W., and Niewold, T.B. (2018). Type I interferon in rheumatic diseases. Nat. Rev. Rheumatol. *14*, 214–228. https://doi.org/10.1038/nrrheum.2018.31.

41. Schmitt, N., Liu, Y., Bentebibel, S.E., Munagala, I., Bourdery, L., Venuprasad, K., Banchereau, J., and Ueno, H. (2014). The cytokine TGF-β2 co-opts signaling via STAT3-STAT4 to promote the differentiation of human TFHcells. Nat. Immunol. *15*, 856–865. https://doi.org/10.1038/ni.2947.

42. Sumida, T.S., Dulberg, S., Schupp, J.C., Lincoln, M.R., Stillwell, H.A., Axisa, P.P., Comi, M., Unterman, A., Kaminski, N., Madi, A., et al. (2022). Type I interferon transcriptional network regulates expression of coinhibitory receptors in human T cells. Nat. Immunol. *23*, 632–642. https://doi.org/10.1038/s41590-022-01152-y.

43. Cunningham, A.F., Gaspal, F., Serre, K., Mohr, E., Henderson, I.R., Scott-Tucker, A., Kenny, S.M., Khan, M., Toellner, K.M., Lane, P.J.L., and MacLennan, I.C.M. (2007). Salmonella induces a switched antibody response without germinal centers that impedes the extracellular spread of infection. J. Immunol. *178*, 6200–6207. https://doi.org/10.4049/jimmunol.178.10.6200.

44. Kalinke, U., Bucher, E.M., Ernst, B., Oxenius, A., Roost, H.P., Geley, S., Kofler, R., Zinkernagel, R.M., and Hengartner, H. (1996). The role of somatic mutation in the generation of the protective humoral immune response against vesicular stomatitis virus. Immunity *5*, 639–652. https://doi.org/10.1016/s1074-7613(00)80277-0.

45. Kalinke, U., Oxenius, A., Lopez-Macias, C., Zinkernagel, R.M., and Hengartner, H. (2000). Virus neutralization by germ-line vs. hypermutated antibodies. Proc. Natl. Acad. Sci. USA *97*, 10126–10131. https://doi.org/10.1073/pnas.97.18.10126.

46. Chen, Y., Tong, X., Li, Y., Gu, B., Yan, J., Liu, Y., Shen, H., Huang, R., and Wu, C. (2020). A comprehensive, longitudinal analysis of humoral responses specific to four recombinant antigens of SARS-CoV-2 in severe and non-severe COVID-19 patients. PLoS Pathog. *16*, e1008796. https://doi.org/10.1371/journal.ppat.1008796.

47. Kofler, D.M., Severson, C.A., Mousissian, N., De Jager, P.L., and Hafler, D.A. (2011). The CD6 multiple sclerosis susceptibility allele is associated with alterations in CD4+ T cell proliferation. J. Immunol. *187*, 3286–3291. https://doi.org/10.4049/jimmunol.1100626.

48. Karakas Celik, S., Cakmak Genc, G., and Dursun, A. (2021). A bioinformatic approach to investigating cytokine genes and their receptor variants in relation to COVID-19 progression. Int. J. Immunogenet. *48*, 211–218. https://doi.org/10.1111/iji.12522.

49. Woodruff, M.C., Ramonell, R.P., Nguyen, D.C., Cashman, K.S., Saini, A.S., Haddad, N.S., Ley, A.M., Kyu, S., Howell, J.C., Ozturk, T., et al. (2020). Extrafollicular B cell responses correlate with neutralizing antibodies and morbidity in COVID-19. Nat. Immunol. *21*, 1506–1516. https://doi.org/10.1038/s41590-020-00814-z.

50. Stuart, T., Butler, A., Hoffman, P., Hafemeister, C., Papalexi, E., Mauck, W.M., III, Hao, Y., Stoeckius, M., Smibert, P., and Satija, R. (2019). Comprehensive integration of single-cell data. Cell *177*, 1888–1902.e21. https://doi.org/10.1016/j.cell.2019.05.031.

51. Giudicelli, V., Chaume, D., and Lefranc, M.P. (2005). IMGT/GENE-DB: a comprehensive database for human and mouse immunoglobulin and T cell receptor genes. Nucleic Acids Res. *33*, D256–D261. https://doi.org/10.1093/nar/gki010.

52. Ye, J., Ma, N., Madden, T.L., and Ostell, J.M. (2013). IgBLAST: an immunoglobulin variable domain sequence analysis tool. Nucleic Acids Res. *41*, W34–W40. https://doi.org/10.1093/nar/gkt382.

53. Gupta, N.T., Vander Heiden, J.A., Uduman, M., Gadala-Maria, D., Yaari, G., and Kleinstein, S.H. (2015). Change-O: a toolkit for analyzing large-scale B cell immunoglobulin repertoire sequencing data. Bioinformatics *31*, 3356–3358. https://doi.org/10.1093/bioinformatics/btv359.

54. Yaari, G., Vander Heiden, J.A., Uduman, M., Gadala-Maria, D., Gupta, N., Stern, J.N.H., O'Connor, K.C., Hafler, D.A., Laserson, U., Vigneault, F., and Kleinstein, S.H. (2013). Models of somatic hypermutation targeting and substitution based on synonymous mutations from high-throughput immunoglobulin sequencing data. Front. Immunol. *4*, 358. https://doi.org/10.3389/fimmu.2013.00358.

55. Cantu, V.A., Sadural, J., and Edwards, R. (2019). PRINSEQ++, a multi-threaded tool for fast and efficient quality control and preprocessing of sequencing datasets. PeerJ Prepr *7*, e27553v1. https://doi.org/10.7287/peerj.preprints.27553v1.

56. Dobin, A., Davis, C.A., Schlesinger, F., Drenkow, J., Zaleski, C., Jha, S., Batut, P., Chaisson, M., and Gingeras, T.R. (2013). STAR: ultrafast universal RNA-seq aligner. Bioinformatics *29*, 15–21. https://doi.org/10.1093/bioinformatics/bts635.

57. Li, B., and Dewey, C.N. (2011). RSEM: accurate transcript quantification from RNA-Seq data with or without a reference genome. BMC Bioinf. *12*, 323. https://doi.org/10.1186/1471-2105-12-323.

58. Love, M.I., Huber, W., and Anders, S. (2014). Moderated estimation of fold change and dispersion for RNA-seq data with DESeq2. Genome Biol. *15*, 550. https://doi.org/10.1186/s13059-014-0550-8.

59. Kuleshov, M.V., Jones, M.R., Rouillard, A.D., Fernandez, N.F., Duan, Q., Wang, Z., Koplev, S., Jenkins, S.L., Jagodnik, K.M., Lachmann, A., et al. (2016). Enrichr: a comprehensive gene set enrichment analysis web server 2016 update. Nucleic Acids Res. *44*, W90–W97. https://doi.org/10.1093/nar/gkw377.

60. Remy, M.M., Alfter, M., Chiem, M.N., Barbani, M.T., Engler, O.B., and Suter-Riniker, F. (2019). Effective chemical virus inactivation of patient serum compatible with accurate serodiagnosis of infections. Clin. Microbiol. Infect. *25*, 907.e7-907907.e12. https://doi.org/10.1016/j.cmi.2018.10.016.

61. Butler, A., Hoffman, P., Smibert, P., Papalexi, E., and Satija, R. (2018). Integrating single-cell transcriptomic data across different conditions, technologies, and species. Nat. Biotechnol. *36*, 411–420. https://doi.org/10.1038/nbt.4096.

62. Nielsen, S.C.A., Yang, F., Jackson, K.J.L., Hoh, R.A., Röltgen, K., Jean, G.H., Stevens, B.A., Lee, J.Y., Rustagi, A., Rogers, A.J., et al. (2020). Human B cell clonal expansion and convergent antibody responses to SARS-CoV-2. Cell Host Microbe *28*, 516–525.e5. https://doi.org/10.1016/j.chom.2020.09.002.

STAR★METHODS

KEY RESOURCES TABLE

REAGENT or RESOURCE	SOURCE	IDENTIFIER
Antibodies		
BV605 anti-human CD3 (clone UCHT1)	Biolegend	300480
BV785 anti-human CD4 (clone SK3)	Biolegend	344642
APCFire750 anti-human CD8 (clone SK1)	Biolegend	344746
BV421 anti-human CD197(CCR7) (clone G043H7)	Biolegend	353208
Alexa Fluor 700 anti-human CD45RA (clone HI100)	BD Biosciences	560673
PE-CF594 anti-human CD25 (clone BC96)	BD Biosciences	567489
PE anti-human PD-1 (cline EH12.2H7)	Biolegend	329906
APC anti-human TIM3 (cline F38-2E2)	Biolegend	345012
BV711 anti-human CD38 (clone HIT2)	Biolegend	303528
BB515 anti-human HLA-DR (clone G46-6)	BD Biosciences	564516
BB700 anti-human CXCR5 (clone RF8B2)	BD Biosciences	566469
PE-Cy7 anti-human CD127 (clone HIL-7R-M21)	BD Biosciences	560822
BV785 anti-human CD19 (clone SJ25C1)	Biolegend	302240
BV421 anti-human CD138 (clone MI15)	Biolegend	356516
Alexa Fluor 700 anti-human CD20 (clone 2H7)	Biolegend	302322
Alexa Fluor 647 anti-human CD27 (clone M-T271)	Biolegend	356434
PE/Dazzle594 ant-human IgD (clone IA6-2)	Biolegend	348240
BB700 anti-human CD183/CXCR3 (clone 1C6/CXCR3)	BD Biosciences	566532
PE-Cy7 anti-human CD86 (clone IT2.2)	Biolegend	305422
APC/Fire750 anti-human IgM (clone MHM-88)	Biolegend	314546
BV605 anti-human CD24 (clone ML5)	Biolegend	311124
Alexa Fluor 647 anti-human CXCR5 (clone RF8B2)	BD Biosciences	558113
BV421 anti-human CD192(CCR2) (clone K036C2)	Biolegend	357209
FITC anti-human CD195(CCR5) (clone J418F1)	Biolegend	359119
Alexa Fluor 647 anti-human CD45RA (clone HI100)	BD Biosciences	560673
Alexa Fluor 488 anti-human CD183/CXCR3 (clone 1C6/CXCR3)	BD Biosciences	558047
BV421 anti-human CD27 (clone M-T271)	Biolegend	356418
BV510 anti-human CD20 (clone 2H7)	Biolegend	302340
BV711 anti-human CD138 (clone MI15)	Biolegend	356522
PE-Cy7 anti-human CD183/CXCR3 (clone 1C6/CXCR3)	BD Biosciences	560831
BV421 anti-human CX3CR1 (clone 2A9-1)	Biolegend	341619
BV421 anti-human LAG3 (clone 11C3C65)	Biolegend	369314

Continued

REAGENT or RESOURCE	SOURCE	IDENTIFIER
FITC anti-human CD186(CXCR6) (clone K041E5)	Biolegend	356019
FITC anti-human CD3 (clone UCHT1)	BD Biosciences	561806
PE-Cy7 anti-human CD4 (clone OKT4)	Biolegend	317414
Ultra-LEAF™ Purified anti-human IFN-γ Antibody (clone B27)	Biolegend	506532
mouse IgG1 k isotype controls (clone MOPC-21)	Biolegend	400102
Purified NA/LE Mouse Anti-Human CD3 (clone UCHT1)	BD Biosciences	555329
Purified NA/LE Mouse Anti-Human CD28	BD Biosciences	555725
Chemicals, peptides, and recombinant proteins		
RPMI 1640 medium	Gibco	11875-085
Fetal Bovine Serum	Gemini	100-106
L-glutamine (200mM)	Gibco	25030-081
Pen Strep	Gibco	15140-122
Enterotoxin Type B from Staphylococcus aureus	LIST BIOLOGICAL LABS INC	122
LPS from E. Coli, TLR4 ligand	NOVUS Biologicals	NBP2-25295
MEGACD40L Protein	Enzo	ALX-522-110-C010
Recombinant Human IL-10 Protein	R&D	217-IL-010/CF
Recombinant Human IL-21 Protein	R&D	8879-IL-050/CF
Recombinant Human IFN-gamma Protein	R&D	285-IF-100/CF
Human TruStan FcX	Biolegend	422302
Live/Dead Fixable Aqua	Thermofisher	L34966
Live/Dead Fixable Near-ID	Thermofisher	L34976
Critical commercial assays		
Human B cell isolation kit	Stemcell Technologies	19054
RNeasy Micro Kit	QIAGEN	74034
SuperScript IV VILO Master Mix	Thermofisher	11756050
TaqMan Fast Univ PCR Master Mix	Applied Biosystems	4352046
Taqman qPCR Probe (CXCR3)	Thermofisher	Hs01847760_s1
Taqman qPCR Probe (CXCR4)	Thermofisher	Hs00607978_s1
Taqman qPCR Probe (CCR2)	Thermofisher	Hs00356601_m1
Taqman qPCR Probe (B2M)	Thermofisher	Hs00187842_m1
IgG (Total) Human Uncoated ELISA Kit	Thermofisher	88-50550-88
Human CXCL13/BLC/BCA-1 DuoSet ELISA kit	R&D	DY801
Human IFNg DuoSet ELISA kit	R&D	DY285
Human IL-10 DuoSet ELISA kit	R&D	DY217B
Human IL-21 DuoSet ELISA kit	R&D	DY8879-05
Human SARS-CoV-2 Spike (Trimer) IgM ELISA Kit	Thermofisher	BMS2325
Human SARS-CoV-2 Spike (Trimer) IgG ELISA Kit	Thermofisher	BMS2324
Anti-SARS-CoV-2 S-RBD protein Human IgG ELISA Kit	Proteintech	KE30003
Anti-SARS-CoV-2 S-RBD protein Human IgM ELISA Kit	Proteintech	KE30004

Continued

REAGENT or RESOURCE	SOURCE	IDENTIFIER
LEGENDplex™ SARS-CoV-2 Neut. Ab Assay	Biolegend	741127
SMART-Seq v4 Ultra Low Input RNA Kit	Takara/Clontech	634898
Nextera XT DNA Library Preparation kit	Illumina	FC-131-1024
Deposited data		
RNA-seq data	This paper	GSE 214624
Software and algorithms		
R Statistical Computing Software (v3.6)	The R Foundation	https://www.r-project.org/
Seurat (v3.2.0)	Stuart et al.[50]	https://satijalab.org/seurat/
IMGT/GENE-DB (v3.1.26)	Giudicelli et al.[51]	https://www.imgt.org/IMGTindex/IMGTgene-db.php
IgBLAST (v.1.15.0)	Ye et al.,[52]	https://www.ncbi.nlm.nih.gov/igblast/
Change-O (v.1.0.0)	Gupta et al.[53]	http://clip.med.yale.edu/changeo/
SHazaM (v1.0.2.999)	Yaari et al.[54]	https://shazam.readthedocs.io/en/stable/
Alakazam (v1.0.2.999)	Gupta et al.[53]	https://alakazam.readthedocs.io/en/stable/
PRINSEQ++ (v1.2)	Cantu et al.[55]	https://github.com/Adrian-Cantu/PRINSEQ-plus-plus
STAR (v2.7.1)	Dobin et al.[56]	https://github.com/alexdobin/STAR
RSEM (v1.3.0)	Li and Dewey.[57]	https://github.com/deweylab/RSEM
DESeq2 (v1.34.0)	Love et al.[58]	https://bioconductor.org/packages/release/bioc/html/DESeq2.html
GraphPad Prism version 7	GraphPad	https://www.graphpad.com/guides/prism/8/user-guide/tips_for_using_prism.htm
Enrichr	Kuleshov et al.[59]	https://maayanlab.cloud/Enrichr/

RESOURCE AVAILABILITY

Lead contact
Further information and requests for resources and reagents should be directed to and will be fulfilled by the lead contact, Tomokazu S. Sumida (tomokazu.sumida@yale.edu).

Materials availability
This study did not generate new unique reagents.

Data and code availability
Single-cell RNA-seq data have been deposited at GEO database under accession code: GSE155224. Bulk RNA-seq data are also available under accession code: GSE214624. This paper does not report original code. Any additional information required to reanalyze the data reported in this paper is available from the lead contact upon request.

EXPERIMENTAL MODELS AND SUBJECT DETAILS

Ethics Statement
This study was approved by the Institutional Review Board at the Yale School of Medicine (FWA00002571, Protocol IDs: 2000027690 and 2000027291REG). Informed consent was obtained from all enrolled patients, healthcare workers, and healthy donors.

Patients and samples
Adult patients (≥18 years old) admitted to Yale-New Haven Hospital, positive for SARS-CoV-2 by RT-PCR from nasopharyngeal and/or oropharyngeal swabs, and able to provide informed consent (surrogate consent accepted) were eligible (Table S1). Individuals with pregnant patients, patients with background hematological abnormalities, patients with autoimmune diseases and patients with a history of organ transplantation and on immunosuppressive agents, were excluded from this study.

For the characterization of T cells and B cells, the flow data deposited in the Yale IMPACT Biorepository study were analyzed as described elsewhere.[3,28] All the patients were admitted between 30 March and 27 May 2020 and hospitalized. No samples had

histories of prior COVID-19 infection nor vaccinations and only the baseline data were analyzed except for the analysis of time kinetics. All the experiments were performed on fresh peripheral blood mononuclear cells (PBMCs), and samples were drawn on the average of 11.8 days after first symptoms. 92 hospitalized patients with COVID-19 and 64 COVID-19-uninfected healthcare workers (HCs) were enrolled. Patients with COVID-19 who required admission to the ICU had been classified as "ICU" and 27.8% of them were expired. The other patients classified as "non-ICU" were all discharged without ICU admission. For the patients who were 90 years-old or older, their ages were protected health information, and '90' was put as the surrogate value for the analyses. HCs were all negative in both PCR and serology tests.

Single cell RNA-seq (scRNA-seq) was performed on cryopreserved PBMC samples of 10 patients with COVID-19 following the same criteria as above and 13 age- and sex-matched controls. All the samples were drawn on the average of 11.7 days after first symptoms. Control samples were already collected before the first report of COVID-19 in 2018. From eight of ten patients with COVID-19, PBMC samples from two different time points had been analyzed. Four patients had been classified as "ICU", who required admission to the ICU with mechanical ventilation, and the other six patients classified as "non-ICU" who were hospitalized, but not admitted to ICU and all discharged, and the same criteria as flow data. We have described the full cohort elsewhere.[5]

All the other experiments which include *in vitro* experiments and bulk RNA-seq were performed with fresh PBMCs at the baseline. Patients were admitted between 21st July 2020 and 24th Sep 2021 and all were immunologically naive except blocking experiments (Figure 4E), which had history of prior SARS-CoV-2 vaccinations.

METHOD DETAILS

Peripheral blood mononuclear cells isolation
PBMCs were prepared from whole blood by Ficoll gradient centrifugation (Histopaque (Sigma) in the Yale IMPACT Biorepository study and Lymphoprep (Stemcell) in other experiments). The PBMC layer was collected into a new 50-mL tube and washed twice with PBS to remove any remaining Lymphoprep/Histopaque. As for scRNA-seq and flow cytometry, the pelleted cells were treated with ACK buffer for red cell lysis. All the other experiments including bulk RNA-seq samples were processed without lysis buffer.

Flow cytometry and sorting
In the Yale IMPACT Biorepository study, the staining was performed mainly in two separate panels for (1) T cell surface staining and (2) B cell surface staining. PBMCs were plated at 1-2 × 10⁶ cells in a 96-well U-bottom plate, and resuspended in Live/Dead Fixable Aqua (ThermoFisher) for 20 min at 4 °C. Following a wash, cells were then blocked with Human TruStan FcX (BioLegend) for 10 min at room temperature. Cocktails of desired staining antibodies were directly added to this mixture for 30 min at room temperature. Before analysis, cells were washed and resuspended in 100 μL of 4% paraformaldehyde for 30 min at 4 °C. We have described the detailed methods elsewhere.[3] Data acquisition had been done, dividing into several times (T cell panel; 32 batches, B cell panel; 19 batches) by the specific flow cytometry (Attune NXT; Thermofisher). They did not contain any specific experiment batches with significant outliers (more than mean +2SD or less than mean – 2SD) than the others. For other experiments, freshly isolated PBMCs were stained with cocktails of desired staining antibodies for 30 min at 4°C. Specific T cell and B cell subsets were sorted on a Sony MA900 cell sorter.

T-B-cell co-culture experiments
Co-culture experiments were performed referenced as described previously.[21] In brief, sorted T cell populations (5000-20000 cells) from PBMCs of patients with COVID-19 were co-cultured with autologous CD20⁺CD27⁺ memory B cells at a ratio of 1:3 in 200 μL of RPMI 1640 medium supplemented with 10% fetal bovine serum (FBS), 2 nM L-glutamine, and 100 U/ml penicillin, 100 μg/mL streptomycin (Gibco), stimulated with SEB (1 μg/mL) and LPS (1 μg/mL) for 7 days. Supernatants were collected, and total IgG (Invitrogen), and cytokine/chemokine levels (R&D systems) were measured by ELISA. Some experiments added anti-human IFNγ antibodies (5 μg/mL) or mouse IgG1 k isotype controls on day 0 and 4 for the neutralization of IFNγ bioactivities. Cells were harvested and analyzed by flow cytometry, with plasma cells defined as CD27^high CD138⁺ cells.

B cell differentiation *in vitro*
We extracted PBMCs from healthy volunteers. After the isolation of CD19⁺ B cells from PBMCs using Human B cell isolation kit (Stemcell Technologies), CD20⁺CD27⁺ memory B cells were sorted on a FACS Aria (BD Biosciences) and stimulated with CD40L (0.05 μg/mL), IL-21 (20 ng/mL) and other cytokines in culture medium the same as above. After 7 days, CD27^high CD138+ plasma cells were sorted for gene expression analysis by qPCR.

T cell stimulation *in vitro*
We extracted PBMCs from patients with COVID-19. Each subset of memory CD4+ T cells based on the expression levels of PD-1 and CXCR5 were stimulated with anti-CD3/CD28 (each 1 μg/mL) for 48 h and cytokine levels were measured by ELISA (all from R&D systems) according to the manufacturer's instructions. 1% Triton X-100 for 60 min at room temperature was added before ELISA to reduce risk from any potential virus in the supernatant.[60]

Quantitative PCR

Total RNA was extracted using RNeasy Micro Kit (QIAGEN) according to the manufacturer's instructions. cDNA was synthesized with SuperScript IV VILO Master Mix (Thermofisher). cDNAs were amplified with Taqman probes (Taqman Gene Expression Arrays) and TaqMan Fast Advanced Master Mix on a StepOne Real-Time PCR System (Applied Biosystems) according to the manufacturer's instructions. The RNA expression was measured relative to *B2M* expression.

The measurement of anti-SARS-CoV-2 antibodies

Sera was collected from patients with COVID-19 and ELISA assays (Proteintech) were performed. In brief, sera were diluted with 1:100 and added to the RBD S-RBD pre-coated plate. After 30 min incubation at room temperature, wells were washed and horseradish peroxidase-conjugated anti-human IgG or IgM were added. After 30 min incubation, wells were washed, followed by TMB reagents. Reagents including sulfuric acid were used to stop reactions and the color intensities were evaluated at 450nm with the correction wavelength set at 630nm. For the evaluation of neutralizing antibodies, sera were diluted with 1:100 and beads-based SARS-CoV-2 neutralizing antibody assay (Biolegend) was used, following the protocol.

Single cell RNA-seq data processing

A PBMC scRNA-seq dataset which had been previously performed and reported by us[5] was reanalyzed. In brief, single cell barcoding of PBMC and library construction had been performed using the 10x Chromium NextGEM 5 prime kit according to manufacturer's instructions. Libraries had been sequenced on an Illumina Novaseq 6000 platform. Raw reads had been demultiplexed and processed using Cell Ranger (v3.1) mapping to the GRCh38 (Ensembl 93) reference genome. Resulting gene-cell matrices had been analyzed using the package Seurat[50,61] in the software R (v3.6.2) including integration of data, clustering, multiplet identification and cell type annotation. We have described the detailed methods elsewhere.[5] PBMCs were processed with four different experiments, and we could not find critical batch differences among experiments. The annotated R object was used for sub-clustering of B cells.

The three cell populations, "Memory B cells", "Naive B cells " and "Plasma cells" in total PBMCs were re-clustered to obtain a finer cell type granularity. To remove batch- and single-donor effects, we integrated all 31 samples of these populations into one dataset using reference-based anchor finding and integration workflow. We chose 2 healthy donor samples (C27 and C32) and 2 COVID-19 samples (NS1B and TS3A), which have enough B cell numbers, as references for anchor finding and integration. The top 2000 variable genes were selected, and integration anchors were determined by "FindIntegrationAnchors" without k.filter for low cell numbers in some samples. These anchors were used to integrate the data using the "IntegrateData" function with top 30 dimensions and scaled. The top 17 PCs were used for data integration and downstream steps, along with a clustering resolution of 0.4. Cluster-specific gene expression profiles were established using the "FindAllMarkers" per cluster and per subset to annotate the clusters. Doublet clusters were determined by co-expression of heterogeneous lineage markers (e.g., *MS4A1* and *CD3*). These clusters were removed prior to finalizing the UMAPs.

B cell receptor repertoire analysis

B cell receptor (BCR) V(D)J repertoire data processing, clonal clustering, and unmutated germline ancestor sequence reconstruction was previously performed.[5] Briefly, V(D)J genes aligned to the IMGT/GENE-DB v3.1.26[51] germline reference database using IgBLAST v.1.15.0.[52] Cells with multiple IGH V(D)J sequences were assigned to the most abundant IGH V(D)J sequence by UMI count, and ties were broken by the first identified heavy chain. Non-functional sequences were removed. V(D)J sequences within each patient were grouped into clonal clusters by first partitioning based on common IGHV gene annotations, IGHJ gene annotations, and junction lengths. Within these groups, sequences differing from one another by a length normalized Hamming distance of 0.15 within the junction region were defined as clones by single-linkage clustering using Change-O v.1.0.0.[53] Germline sequences were reconstructed for each clone with the D segment and N/P regions masked (replaced with "N" nucleotides) using the CreateGermlines.py function within Change-O v.1.0.0.

Somatic hypermutation frequency was calculated using SHazaM v1.0.2.999[54] as the frequency of non-ambiguous nucleotide differences along the IGHV gene segment (IMGT positions 1–312) between each sequence and its inferred germline ancestor. To identify unmutated B cell clones of different cell types and isotypes, B cell clones were separated by cell type and isotype and considered "unmutated" if the median somatic hypermutation frequency of their constituent sequences was <1%. This cutoff was also used in.[5,62] To quantify B cell clonal diversity, we calculated Simpson's diversity within each patient for plasmablast subsets using the alphaDiversity function of Alakazam v1.0.2.999.[53] To account for differences in sequence depth, the number of sequences within each patient were down-sampled to the same number of sequences, and the mean of 100 such re-sampling repetitions was reported. Only patients with at least 30 B cells were included in diversity calculations. All statistical analyses of BCR sequences were performed with R (v3.6.1).

Bulk RNA-seq

cDNA and library preparation and sequencing

RNAs were isolated using RNeasy Plus Micro Kit (QIAGEN) and cDNAs were generated using the SMART-Seq v4 Ultra Low Input RNA Kit for sequencing (Takara/Clontech). Barcoded libraries were generated by the Nextera XT DNA Library Preparation kit (Illumina) and sequenced with a 2x100 bp paired-end protocol on the HiSeq 4000 Sequencing System (Illumina).

Bulk RNA-seq data analysis

Low quality ends (less than phred score = 30) and short read length (minimum length = 30) was trimmed using PRINSEQ++[55] (version1.2). Trimmed reads were aligned to the hg38 genome reference using STAR[56] (v2.7.1), and subsequently RSEM (RNA-Seq by Expectation Maximization)[57] was used to count reads mapping to the genes from Ensembl release 93. We applied limma to model each gene as a linear combination of donor-specific effects. Top 1000 genes by variance were analyzed for PCA. Heat maps show row-normalized relative gene expression z-scores across columns. Pairwise differential expression was performed using the R package DESeq2.[58] The cutoff value to select differentially expressed genes is provided in each figure legend.

Pathway analysis

The differentially expressed genes upregulated in PD-1^{high}CXCR5$^-$CD4$^+$ T cells compared with PD-1^{high}CXCR5$^+$CD4$^+$ T cells were inputted to Enrichr[59] to calculate enrichment of pathway-associated terms.

QUANTIFICATION AND STATISTICAL ANALYSIS

All statistical analyses were performed using R or GraphPad Prism 7 (GraphPad Software). Detailed information about statistical analysis, including tests and values used, is provided
  in the figure legends.